



High-order Variational Multiscale Model with an Explicit Filtering in a Stabilised Finite Element Method for LES/DES Computations

Pierre Yser*, Sébastien Barré†, Frédéric Chalot‡, and Franck Dagrau†

Dassault Aviation

78, quai Marcel Dassault – 92552 Saint-Cloud CEDEX – France

Christophe Bailly‡

Centre Acoustique, École Centrale de Lyon & LMFA UMR CNRS 5509

36, avenue Guy de Collongue – 69134 Écully CEDEX – France

Flow steadiness is often overpredicted near the wall by *Detached-Eddy Simulation (DES)*. This problem is here addressed with a *Streamline Upwind Petrov-Galerkin (SUPG)* finite element method. An hybrid *Variational MultiScale (VMS)* model is implemented to enhance the *Large-Eddy Simulation (LES)* mode of DES computation. An explicit filtering method is developed in order to compute the filtered field involved in a VMS model. Furthermore, these VMS fluctuations are also used to improve unsteadiness in the area close to the walls. This approach is assessed with the Taylor-Green vortices and finally applied to the LEISA II configuration.

Key Words : *High-order finite elements, SUPG, VMS, DES, Explicit Filtering, Taylor-Green vortices, Slat noise*

Nomenclature

$\underline{\mathbf{U}}$	Conservative variables	f_c	Clipping function
$\underline{\mathbf{V}}$	Entropic variables	K	Kinetic energy
$\underline{\mathbf{A}}_0$	Change of variable matrix	ϵ	Dissipation
$\underline{\mathbf{A}}_i$	Jacobian matrix of Euler flux	ν	Kinematic viscosity
$\underline{\mathbf{K}}_{ij}$	Diffusive matrix	<i>Superscript :</i>	
ρ	Mass density (kg/m ³)	R	Resolved field
$\underline{\mathbf{u}}$	Velocity (u,v,w) (m/s)	'	Underscale field
T	Temperature (K)	~	Field low frequency
p	Pressure (Pa)	"	Field high frequency
N_a	Interpolation function	a	Node value
$\underline{\tau}$	Stabilisation matrix	e	Element value
$\underline{\mathbf{x}}$	Spatial coordinates (m)	<i>Subscript :</i>	
$\underline{\mathbf{k}}$	Spectral wave number	VMS	VMS variable
Ω	Volume (m ³)	DES	DES variable
Δ	Mesh length (m)		

*PhD Student at Dassault Aviation & LMFA Acoustic Laboratory / Ecole Centrale de Lyon

†Research Engineer at Dassault Aviation

‡Professeur des Universités, École Centrale de Lyon & LMFA UMR CNRS

I. Introduction

Direct Navier-Stokes Simulation (DNS) still requires too heavy computational resources to be applied on a complex industrial configuration whereas *Reynolds Averaged Navier-Stokes* (RANS) models are not accurate enough to predict unsteadiness at the limit of the flight envelope and various acoustic phenomena. *Large Eddy Simulation* (LES) provides a theoretical framework to filter Navier-Stokes equations by decomposing the unsteady flow between resolved scales and small modelled subgrid structures. But LES may be still too costly for complex industrial applications. In order to bypass the near wall mesh constraints, *Detached-eddy Simulation* (DES) approaches such as the Spalart-Allmaras based model [43] are often preferred. Advantages of RANS robustness close to the wall are combined with LES accuracy in areas of separated flows. In terms of modelling, DES behaves as a classical Smagorinsky LES but tends to an *Unsteady Reynolds Averaged Navier Stokes* (URANS) simulation near the wall. Various studies already deal with the most recent formulation of DES namely *Delayed Detached eddy Simulation* (DDES) model, refer to [36, 38, 42] among others.

Improvements in flow description are however needed. As an illustration, the determination of the fluctuating flow near the wall is required in aeroacoustic applications to compute the acoustic far field from Curle's formulation [9]. In the matter of fact the URANS modelling can become a serious problem for unsteadiness in areas of interest. Fluctuations are too much filtered in URANS simulation and numerical problems appear in case of detached flows or for the spatial development of a shear layer [11, 40]. Various methods have led to improve DDES, sometimes in a sophisticated way, see the review by Deck [11] for example. This formulation is currently used at Dassault Aviation. How to increase the spatial accuracy of a simulation and its unsteadiness feature near the wall by keeping a reasonable number of points without increasing computational costs? It appears that improving the LES modelling itself may lead to a significant improvement in the flow resolution [49].

The fidelity of such simulations is addressed in the present work by examining two aspects which are intrinsically coupled, the subgrid model [7, 19] and the order of the numerical schemes [6, 8, 12]. The first point has been addressed by various studies by updating the URANS area or the definition of the DDES coefficients as the definition of the subgrid length scale [40] for instance. But still, the equivalent classical Smagorinsky LES model is known to be too much dissipative at least for transitional flows. This problem can be solved by using an alternative LES model for which filter transfer function applied to the turbulent flow is not a low pass filtering. These kinds of model are known as *Variational Multi-Scale* (VMS) refer to [23–26, 29, 38]. The second point seems to be promising for future simulations. There are different advantages and two of them are especially appealing. It is straightforward to implement in finite element formulation and more efficient in terms of CPU time than increasing the number of grid points for a given accuracy. The wall unsteadiness problem is more complex to tackle. In the present study, a VMS method involving an explicit filtering [31, 35, 37] has been developed. Furthermore the introduction of a clipping function in the wall region helps to reduce the URANS zone by introducing VMS fluctuations.

The paper is organised as follows. First, the numerical tools to solve the VMS problem using a finite element high-order code are introduced. The entropic formulation of the *Galerkin least-square formulation* (GLS) finite element method is also briefly described. Secondly, the original implementation of VMS and filtering process in the in-house entropic finite element Dassault Aviation code is presented. This originality comes from the explicit filtering in finite elements for an entropic simulation, especially for spatial high orders. Thirdly the Taylor-Green vortices is solved to assess the new VMS developments in LES mode. Finally a slat noise benchmark will illustrate a fully realistic simulation and the benefits of this method.

II. Numerical method

A. Navier-Stokes equations in entropic formulation

The flow is assumed to be compressible and air is considered a perfect gas in local thermodynamic equilibrium. The bulk viscosity is neglected and the thermal conduction verifies the Fourier's law. The Navier-Stokes equation can be rewritten in matrix form as follow

$$\underline{\mathbf{U}}_{,t} + \underline{\mathbf{A}}_i \underline{\mathbf{U}}_{,i} = (\underline{\mathbf{K}}_{ij} \underline{\mathbf{U}}_{,j})_{,i}$$

where $\underline{\mathbf{U}}$ represents the conservative variables, $\underline{\mathbf{A}}_i = \underline{\mathcal{F}}_{i,\underline{\mathbf{U}}}$ is the i^{th} Jacobian matrix of Euler flux and $\underline{\mathbf{K}}_{ij}$ is the diffusive matrix defined as $\underline{\mathbf{K}}_{ij} \underline{\mathbf{U}}_{,j} = \underline{\mathcal{F}}^{\text{diff}}$. The index starting with a coma denotes partial derivatives.

These matrices are defined from the following vectors

$$\underline{\mathbf{U}} = \rho \begin{pmatrix} 1 \\ u_1 \\ u_2 \\ u_3 \\ E_t \end{pmatrix}; \quad \underline{\mathcal{F}}_i = \begin{pmatrix} \rho u_i \\ \rho u_i u_1 + p \delta_{1i} \\ \rho u_i u_2 + p \delta_{2i} \\ \rho u_i u_3 + p \delta_{3i} \\ \rho u_i E_t + p u_i \end{pmatrix}; \quad \underline{\mathcal{F}}^{\text{diff}} = \begin{pmatrix} 0 \\ \sigma_{1i}^{\text{D}} \\ \sigma_{2i}^{\text{D}} \\ \sigma_{3i}^{\text{D}} \\ \sigma_{ji}^{\text{D}} u_i - q_j^T \end{pmatrix}$$

with ρ the density, u_i the velocity in the i^{th} direction, E_t the total energy, δ the Dirac function, q_j^T the thermal flux, $\underline{\sigma}^{\text{D}}$ the deviatoric part of the stress tensor $\underline{\sigma}^{\text{D}} = 2\mu\underline{\mathbf{S}}^{\text{D}}$ and $\underline{\mathbf{S}}^{\text{D}}$ the deviatoric part of the strain tensor defined as $\underline{\mathbf{S}}^{\text{D}} = \underline{\mathbf{S}} - 1/3\text{tr}(\underline{\mathbf{S}})\underline{\mathcal{I}}$ where $\underline{\mathbf{S}} = 1/2(\underline{\text{grad}}(\mathbf{u}) + \underline{\text{grad}}(\mathbf{u})^T)$ is the symmetrical part of the strain tensor, $\underline{\mathcal{I}}$ the identity matrix and μ the dynamic viscosity.

This formulation is not well suited for numerical simulations in finite elements. The entropic formulation is preferred because the problem can be recasted into symmetrical and positive definite matrices. By considering the change of variable $\mathcal{H}(\underline{\mathbf{U}}) = -\rho s$ where the definition of \mathcal{H} can be found in Mallet [32], the problem can be reformulated as follow

$$\underline{\tilde{\mathbf{A}}}_0 \mathbf{V}_{,t} + \underline{\tilde{\mathbf{A}}}_i \mathbf{V}_{,i} = \left(\underline{\tilde{\mathbf{K}}}_{ij} \mathbf{V}_{,j} \right)_{,i} \quad (1)$$

where $\underline{\tilde{\mathbf{A}}}_0$ is the change of variable matrix and \mathbf{V} is defined by

$$\mathbf{V} = \frac{1}{T} \begin{pmatrix} h - Ts - \frac{\|\mathbf{u}\|^2}{2} \\ u_1 \\ u_2 \\ u_3 \\ -1 \end{pmatrix}$$

where s is the entropy, h the enthalpy and T the temperature.

B. Finite element resolution

A general presentation on finite element method can be found in Hughes [21], Carey et Oden [5], Strang et Fix [44] and Zienkiewicz [50]. The Dassault Aviation code called **AETHER** is described in references [29,32,39]. The main algorithm steps are introduced in this section.

1. Variational formulation and GLS formulation

The variational formulation of Eq.(1) is obtained by multiplying this equation with the weighting functions $\underline{\mathbf{W}}$ taken in the same functional space as \mathbf{V} . This yields

$$\int_{\Omega} \underline{\mathbf{W}} \cdot \left(\underline{\tilde{\mathbf{A}}}_0 \mathbf{V}_{,t} + \underline{\tilde{\mathbf{A}}}_i \mathbf{V}_{,i} - \left(\underline{\tilde{\mathbf{K}}}_{ij} \mathbf{V}_{,j} \right)_{,i} \right) d\Omega = 0 \quad (2)$$

where $\underline{\tilde{\mathbf{A}}}_0 \mathbf{V}_{,t} + \underline{\tilde{\mathbf{A}}}_i \mathbf{V}_{,i} - \left(\underline{\tilde{\mathbf{K}}}_{ij} \mathbf{V}_{,j} \right)_{,i}$ is defined as the residual part of Eq.(2) and Ω denotes the volume of the computational domain.

The Navier-Stokes equations are known to be numerically unstable with a finite element formulation, refer to [20,22,32]. To fix this well-established problem, a perturbation is added to the weighting functions $\underline{\mathbf{W}}$, taking the form

$$\underline{\mathbf{W}} \Rightarrow \underline{\mathbf{W}} + \underline{\mathcal{I}} \underline{\mathcal{L}}(\underline{\mathbf{W}})$$

where $\underline{\mathcal{L}} = \underline{\tilde{\mathbf{A}}}_i \partial / \partial \mathbf{x}_i - \left(\underline{\tilde{\mathbf{K}}}_{ij} \partial / \partial \mathbf{x}_i \right)_{,i}$ is the Navier-Stokes operator of Eq.(1). To balance the convection, an artificial dissipation is added to the equation by the mean of the stabilisation matrix $\underline{\mathcal{I}}$ which is based on the

eigenvalues of $\tilde{\underline{\mathbf{A}}}_0$, $\tilde{\underline{\mathbf{A}}}_i$ and $\tilde{\underline{\mathbf{K}}}_{ij}$. The aim is to correct the unbalanced convection solved in Galerkin method numerical scheme, by comparing this term to the overall dissipation of the computation. The stabilisation matrix is only defined locally on the elements from finite element method. Despite its local definition, the stabilisation has a global impact on the numerical solution. These matrices are multiplied by the residual part of Eq.(2) to keep the consistency of the solution. The stabilised equations of the entropic formulation are then given by

$$\int_{\Omega} (\underline{\mathbf{W}} + \underline{\tau} \underline{\mathcal{L}}(\underline{\mathbf{W}})) \cdot (\tilde{\underline{\mathbf{A}}}_0 \underline{\mathbf{V}}_{,t} + \underline{\mathcal{L}}(\underline{\mathbf{V}})) d\Omega = 0$$

The *Streamline Upwind Petrov-Galerkin* (SUPG) stabilisation is obtained by neglecting the diffusive term of the weighting functions, and is implemented in AETHER .

2. Space discretisation

Eq.(2) is then projected on the space of the interpolation functions. These functions are noted N_a , where a represents the node number. Lagrangian polynomials N_a are used, taken the value 1 at one point of the mesh and 0 otherwise, that is

$$N_a(\underline{\mathbf{x}}_b) = \delta_{ab} = \begin{cases} 1 & \text{if } a = b \\ 0 & \end{cases}$$

To improve the numerical order of the space discretisation, it must be recognised that only the polynomial order of the interpolation functions needs to be increased as illustrated Fig.1.

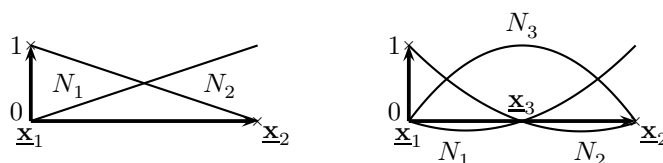


Figure 1. Interpolation functions of order 2 on the left and order 3 on the right for a one dimensional domain

Finite elements used in this work are iso-parametrical and symmetrical. As the result, the same interpolation functions are thus used to interpolate the space coordinates $\underline{\mathbf{x}}$. These interpolation functions are thus called shape functions. The Jacobian matrices involved in metrics can be easily calculated thanks to

$$\begin{cases} \underline{\mathbf{V}} &= \sum_a N_a(\underline{\mathbf{x}}) \underline{\mathbf{V}}(a) \\ \underline{\mathbf{x}} &= \sum_a N_a(\underline{\mathbf{x}}) \underline{\mathbf{x}}_a \end{cases}$$

These symmetrical elements have flat faces and nodes at equal distance from each others. This helps to obtain an easier algorithmic implementation because the Jacobian is then constant. Space differentiation is straightforward inside the element. Moreover these hypothesis help to better understand and control transfer function of the filtering because polynomial interpolation functions in the reference element stay polynomial in the real element.

C. VMS and entropic finite element

The Navier-Stokes equations are filtered in space in LES. This leads to the introduction of additional terms. These so-called subgrid-scale terms represent interactions with the missing scales and need to be modeled. Among all these terms, the velocity subgrid-scale tensor $\underline{\underline{\mathbf{T}}}_s$ is dominant (see Erlebacher and Vreman [13, 37, 46]). If $\underline{\mathbf{U}}^R$ is the resolved unknown vector, the filtered Navier-Stokes equations are

$$\underline{\mathbf{U}}_{,t}^R + \underline{\underline{\mathbf{A}}}_i^R \underline{\mathbf{U}}_{,i}^R = \left(\underline{\underline{\mathbf{K}}}_{ij}^R \underline{\mathbf{U}}_{,j}^R \right)_{,i} + \underline{\underline{\mathbf{T}}}_s$$

The simplest closure for $\underline{\underline{\mathbf{T}}}_s$ is provided by the Smagorinsky model [41]. Only dissipation effects based on the functional form of the deviatoric part of the strain tensor are considered. The Smagorinsky model based on a turbulent viscosity is expressed as

$$\begin{cases} \underline{\underline{\mathbf{U}}}_{,t} + \underline{\underline{\mathbf{A}}}_i^R \underline{\underline{\mathbf{U}}}_{,i} = \left(\underline{\underline{\mathbf{K}}}_{ij}^R (\nu, \underline{\underline{\mathbf{U}}}) \underline{\underline{\mathbf{U}}}_{,j} \right)_{,i} + \left(\underline{\underline{\mathbf{K}}}_{ij}^R (\nu_t, \underline{\underline{\mathbf{U}}}) \underline{\underline{\mathbf{U}}}_{,j} \right)_{,i} \\ \nu_t = (C_S \Delta_m)^2 \sqrt{2 \underline{\underline{\mathbf{S}}}^D (\underline{\underline{\mathbf{U}}}) : \underline{\underline{\mathbf{S}}}^D (\underline{\underline{\mathbf{U}}})} \end{cases}$$

where the value of the constant C_S is about 0.1 (see [1,2,30,37]) and ":" defines the matrix product which sum the product of each coefficients of the matrices such as $\underline{\underline{\mathbf{A}}} : \underline{\underline{\mathbf{B}}} = \sum_{ij} A_{ij} B_{ij}$. This model is known to be much dissipative. Indeed, the diffusive flux intensity is determined with the whole resolved field $\underline{\underline{\mathbf{U}}}$ depending of the mesh implicit filtering. Moreover, this flux is applied on the whole resolved spectrum because of the diffusive matrix multiplication by the gradient resolved field. All the large structures of the flow impact and are impacted by the energy transfer at the cut-off wave number because of the Laplacian functional form. Several models like the selective Smagorinsky (see David [10]) and the dynamic Smagorinsky (see Germano [17,18]) try to decrease the value of ν_t i.e. the diffusive flux intensity or to clip the model in selected areas. But still without addressing the spectral effect of the model.

In order to address this problem, a VMS model is introduced. The aim is to decrease the velocity spectral composition used for the subgrid-scale model. In this purpose, the largest scales $\underline{\underline{\mathbf{U}}}$ need to be cut apart of the smallest scales $\underline{\underline{\mathbf{U}}}'$ from the resolved field $\underline{\underline{\mathbf{U}}}$ (see Fig.2).

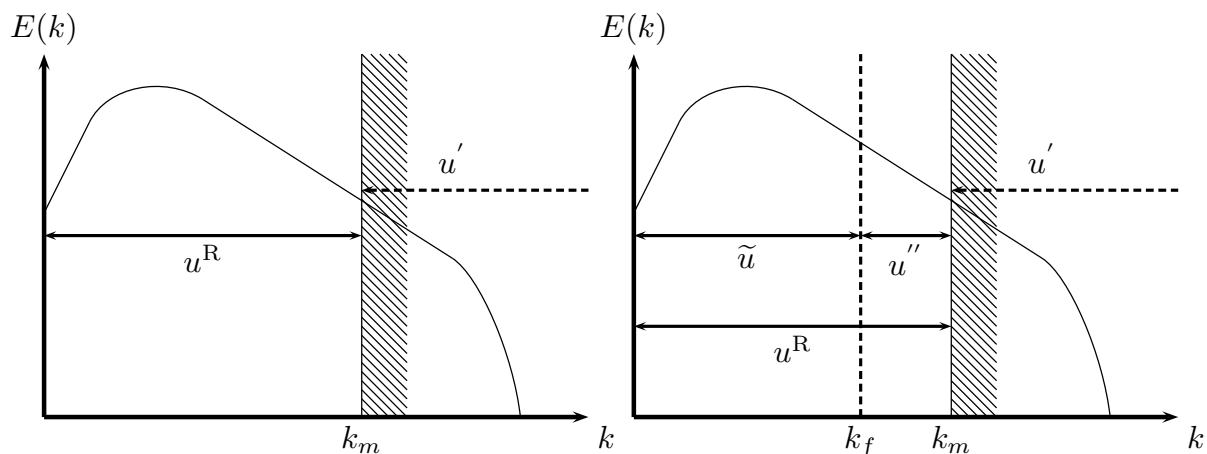


Figure 2. VMS methodology : on the left side a classical LES method, on the right side the separation of VMS resolved scales. k_m is the mesh cut-off wave number and k_f is the filter cut-off wave number

The Smagorinsky like model based on smallest scales is called VMS Small-Small (see Levasseur [29]). Two benefits can be mentioned. Firstly, it changes the functional form of the modelling and impacts only the high wave numbers (act like hyperviscosity models). Secondly, it changes the local intensity of the turbulent viscosity to be adapted to the real presence of subgrid structures and to the mesh refinement. The model is

rewritten in the following form

$$\left\{ \begin{array}{l} \underline{\mathbf{U}}_{,t}^{\text{R}} + \underline{\mathbf{A}}_i^{\text{R}} \underline{\mathbf{U}}_{,i}^{\text{R}} = \left(\underline{\mathbf{K}}_{ij}^{\text{R}} \left(\nu, \underline{\mathbf{U}}^{\text{R}} \right) \underline{\mathbf{U}}_{,j}^{\text{R}} \right)_{,i} + \left(\underline{\mathbf{K}}_{ij}^{\text{R}} \left(\nu_t, \underline{\mathbf{U}}'' \right) \underline{\mathbf{U}}_{,j}'' \right)_{,i} \\ \nu_t = (C_{\text{VMS}} \Delta_m)^2 \sqrt{2 \underline{\mathbf{S}}^{\text{D}} \left(\underline{\mathbf{U}}'' \right) : \underline{\mathbf{S}}^{\text{D}} \left(\underline{\mathbf{U}}'' \right)} \\ C_{\text{VMS}} \Delta_m \approx C_S \Delta_f \left[\left(\frac{\Delta_f}{\Delta_m} \right)^{\frac{4}{3}} - 1 \right]^{-\frac{3}{4}} \\ \underline{\mathbf{U}}'' = \rho \begin{pmatrix} 1 \\ u_1'' \\ u_2'' \\ u_3'' \\ E_t \end{pmatrix} \end{array} \right.$$

where Δ_f and Δ_m are respectively the length of the filter and the length of the element. The coefficient C_{VMS} can be dynamically determined by following the same method as Lilly [30].

The computation of each length scales can be done with several modellings. For an isotropic mesh $\Delta_{\text{vol}} = \sqrt[3]{\Omega^e}$ can be used. But most of the time, some informations of the flow is used in the definition of Δ in order to adapt it to flow physics. For instance, Δ_w is based on a projection of the length scale in the vorticity direction. Recently other Δ modellings have been introduced in order to decrease the mesh anisotropy effect on DES models. For a recent example see [40]. Because the VMS model is used in a LES mode, Δ_m and Δ_f will be computed respectively with the Δ_{vol} method based on the element volume Ω^e and on the macro element volume Ω^M shown in Fig.3. This last one is defined as the element built on each element which share a common node. The Δ definition question for the VMS is still open but the choice made is motivated by the fact that the VMS performs away from the wall where the mesh is chosen unstructured but isotropic.

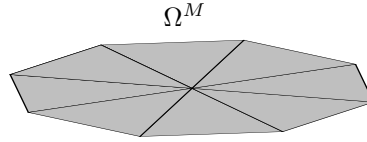


Figure 3. 2D macro element definition Ω^M

The definition of the VMS problem in entropic formulation is obtained through the same way. However, the filtered part of $\underline{\mathbf{V}}$ doesn't represent the low frequencies of the field. Indeed, the entropic change of variable is nonlinear. The entropic problem is finally formulated as follow

$$\left\{ \begin{array}{l} \tilde{\underline{\mathbf{A}}}_0^{\text{R}} \underline{\mathbf{V}}_{,t}^{\text{R}} + \tilde{\underline{\mathbf{A}}}_i^{\text{R}} \underline{\mathbf{V}}_{,i}^{\text{R}} = \left(\tilde{\underline{\mathbf{K}}}_{ij}^{\text{R}} \left(\nu, \underline{\mathbf{V}}^{\text{R}} \right) \underline{\mathbf{V}}_{,j}^{\text{R}} \right)_{,i} + \left(\tilde{\underline{\mathbf{K}}}_{ij}^{\text{R}} \left(\nu_t, \underline{\mathbf{V}}'' \right) \underline{\mathbf{V}}_{,j}'' \right)_{,i} \\ \nu_t = (C_{\text{VMS}} \Delta_m)^2 \sqrt{2 \underline{\mathbf{S}}^{\text{D}} \left(\underline{\mathbf{V}}'' \right) : \underline{\mathbf{S}}^{\text{D}} \left(\underline{\mathbf{V}}'' \right)} \\ C_{\text{VMS}} \Delta_m \approx C_S \Delta_f \left[\left(\frac{\Delta_f}{\Delta_m} \right)^{\frac{4}{3}} - 1 \right]^{-\frac{3}{4}} \\ \underline{\mathbf{V}}'' = \frac{1}{T^{\text{R}}} \begin{pmatrix} T^{\text{R}} V_1^{\text{R}} \\ u_1'' \\ u_2'' \\ u_3'' \\ -1 \end{pmatrix} \end{array} \right. \quad (3)$$

In order to get the filtered field, two methods can be used. Firstly, computing two solutions with one on a coarser mesh and secondly extracting the filtered field from the resolved field by using an explicit filtering method. The last solution has been chosen because of the lower numerical cost. Moreover, the introduction of an explicit filter allows to have partial control on the model spectral band.

D. VMS explicit filter

1. Filtering method in finite elements

Different filtering methods have been developed in the literature. Differential filters (see Sagaut [37]), Fourier's transform filters (see Vasilyev [47]) or interpolation filters (see Mavriplis [4]) are some of them. All these filtering methods are locally equivalent for the AETHER finite element approach. But in order to have an efficient model, the interpolation filters has been chosen. This filtering method avoids a costly global inversion of a mass matrix. But it's local definition on the element can introduce numerical errors and filter approximations.

On the other hand, a classical resolution of an equivalent differential filter is more accurate but costly. Indeed, a differential filter is about solving field gradients which define the order of the filtering. If the filtered field is not properly solved, the gradients computation can destabilise the computation. Field gradients are severely discontinuous with increasing orders and Laplacian elements. This can induce a compulsory averaging and can be costly for the computation. Furthermore, if the simulation order increase, the explicit filtering doesn't improve automatically. In order to reach the effect of a higher filtering order, more complex gradients have to be computed, loading once more the computational cost.

The piecewise polynomial evolution helps to address a new way to solve the filtering problem. Our method is based on the same idea as Brazell *et al* [4]. A classical filtering process is to interpolate the local solution of higher order with the lower order solution .

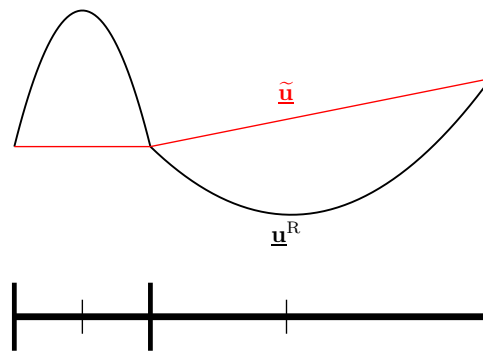


Figure 4. Interpolation filtering of simulation order 3 by linear interpolation function

In Fig.4, the local filtering field $\tilde{\mathbf{u}}$ of the resolved order 3 velocity field \mathbf{u}^R can be easily estimated with a linear interpolation. Indeed this approach is equivalent to the local differential approach with different coefficients because locally the evolution of the field is polynomial, thus the gradient of an order 2 polynomial is a linear one.

This filtering method is well suited to the finite elements because it's really cheap in computational cost. Indeed, only linear interpolation functions need to be added to the computation, and the interpolation is only done on the summits of the higher order elements. Moreover, with the increasing order of the simulation, the equivalent filter will naturally improve. For instance, this filter is equivalent to an order 2 spectral filter for a spatial order 4 simulation.

2. Implementation of the VMS in finite elements

An hybrid approach is used to create an interface between the near-wall treatment and the LES mode (see [27, 45, 48] for several hybrid methods). Fluctuations of the VMS need to be introduced smoothly in the URANS zone of the DDES model. The clipping function used here is based on the f_d function of the Spalart DDES model [42]. Indeed, it is well suited to determine if the gradients are too strong to introduce VMS or if the area is too close to the wall. The f_d function is the following

$$\begin{cases} f_d &= 1 - \tanh \left[(8r_d)^3 \right] \\ r_d &= \frac{\nu_t + \nu}{\sqrt{u_{i,j} u_{j,i}} \kappa^2 d^2} \end{cases}$$

where d is the distance to the wall and κ is taken equal to 0.41. When f_d tends to 0 the simulation should keep the correct prediction of URANS near the wall and when f_d tends to 1 the VMS should introduce the needed fluctuations. But to preserve a good near-wall treatment, the fluctuations shouldn't go too deep in the boundary layer. Finally the hybrid function f_c is chosen like

$$f_c = \begin{cases} 0 & \text{if } f_d < \alpha_i \\ \frac{f_d - \alpha_i}{\alpha_s - \alpha_i} & \text{if } f_d \in [\alpha_i, \alpha_s] \\ 1 & \text{if } f_d > \alpha_s \end{cases}$$

where $\alpha_s > \alpha_i$ in $[0, 1]$ help to adapt the transition from DES to LES. In this paper the following values are used : $\alpha_s = 0.9$ and $\alpha_i = 0.5$. This transition function is then applied at each variables defining the model, *i.e* the turbulent viscosity ν_t , the velocity field \mathbf{u} and the gradient of the entropic variables $\frac{\partial \mathbf{V}^e}{\partial \mathbf{x}}$. The transition is chosen linear for a simpler implicitation and thus take the following shape

$$\begin{cases} \mathbf{u}^{e''}(a) & = (1 - f_c) \mathbf{u}^{e''}(a) + f_c \mathbf{u}^{eR}(a) \\ \frac{\partial \mathbf{V}^{e''}(a)}{\partial \mathbf{x}} & = (1 - f_c) \frac{\partial \mathbf{V}^{e''}(a)}{\partial \mathbf{x}} + f_c \frac{\partial \mathbf{V}^{eR}(a)}{\partial \mathbf{x}} \\ \nu_t^{\text{VMS}} & = (1 - f_c) \nu_t^{\text{VMS}} + f_c \nu_t^{\text{DES}} \end{cases} \quad (4)$$

III. Taylor-Green vortices test case

A. Presentation

The Taylor-Green vortices are an academic flow configuration which enables to study dissipation mechanisms induced by the model in LES mode (see Fauconnier [14]). There is no analytical solution but accurate DNS solutions can be calculated and used as a reference solution. The homogeneous flow slowly turns to be turbulent with a peak of dissipation. The initial conditions are given by

$$\begin{cases} u_1(\mathbf{x}, t) & = u_0 \sin\left(\frac{x}{L_0}\right) \cos\left(\frac{y}{L_0}\right) \cos\left(\frac{z}{L_0}\right) \\ u_2(\mathbf{x}, t) & = u_0 \cos\left(\frac{x}{L_0}\right) \sin\left(\frac{y}{L_0}\right) \cos\left(\frac{z}{L_0}\right) \\ u_3(\mathbf{x}, t) & = 0 \\ p(\mathbf{x}, t) & = p_0 + \frac{\rho_0 u_0^2}{16} \left(\cos\left(\frac{2x}{L_0}\right) + \cos\left(\frac{2y}{L_0}\right) \right) \left(\cos\left(\frac{2z}{L_0}\right) + 2 \right) \end{cases} \quad (5)$$

with $u_0 = 100$ m/s, $p_0 = 10^5$ Pa, $\rho_0 = 1.2$ kg/m³ and $L_0 = 2$ m. Brachet *et al* [3] introduced this generalised Taylor-Green vortices as a periodic three-dimensional flow governed by incompressible Navier-Stokes equation. The flow presents 3D symmetries and is identical on each cubes $\pi L_0 \times \pi L_0 \times \pi L_0$. The flow could be studied on one little cube without adding energy by using periodic conditions. The computational domain chosen is $(x, y, z) \in [0, 2\pi]^3$. The present simulations are performed with the compressible AETHER solver. This is not an issue with respect to the Mach number of the simulation, $M = u_0/L_0 \leq 0.3$. This flow becomes turbulent for a Reynold number $Re_{L_0} = u_0 L_0 \rho_0 / \mu$ higher than 500. The Reynolds number is chosen to be 1500 and correspond to the value of the DNS by Fauconnier [14]. In this configuration, the minimal number of points in each direction to solve correctly the DNS is $N = 256$ and the time step $\Delta t = 5.10^{-3}$ seconds.

In this paper, two meshes are used on a same box of length 2π meters, *i.e* $L_0 = 2$ m. The first mesh is the DNS mesh used to compare AETHER DNS results with the Fauconnier's ones. It is a structured regular mesh with $N = 256$. The second mesh is the LES mesh used to study LES models. It is structured and has $N = 64$ points per direction.

Two quantities are more specifically examined, the dissipation and the kinetic energy. They are made dimensionless by the quantities $t_c = L_0/u_0$ for the time t , u_0^2 for the kinetic energy K and u_0^2/t_c for the dissipation. The kinetic energy K is classically calculated in the volume as

$$K = \frac{1}{\rho_0 \Omega} \int_{\Omega} \rho \frac{\mathbf{u} \cdot \mathbf{u}}{2} d\Omega$$

whereas the dissipation is obtained as the temporal derivative of K

$$\epsilon^T = -\frac{\partial K}{\partial t}$$

This total dissipation can be split into 3 different contributions. First the resolved dissipation ϵ^R , based on the resolved scales in LES

$$\epsilon^R = 2\frac{\nu}{\rho_0\Omega} \int_{\Omega} \rho \underline{\underline{\mathbf{S}}}^D(\underline{\mathbf{u}}^R) : \underline{\underline{\mathbf{S}}}^D(\underline{\mathbf{u}}^R) d\Omega$$

The second dissipation is associated with the subgrid scale model, and is noted ϵ'' . It can be computed with

$$\epsilon'' = \frac{2}{\rho_0\Omega} \int_{\Omega} \rho \nu_t(\underline{\mathbf{u}}'') \underline{\underline{\mathbf{S}}}^D(\underline{\mathbf{u}}'') : \underline{\underline{\mathbf{S}}}^D(\underline{\mathbf{u}}'') d\Omega$$

In a perfect LES simulation, ϵ'' is the strict complement of ϵ^R to obtain ϵ^T . Unfortunately, the stabilisation and numerical errors are also introduced. This last contribution denoted ϵ^N can't be easily expressed, but it can be obtained by considering the balance equation

$$\epsilon^T = \epsilon^R + \epsilon'' + \epsilon^N$$

This last dissipation is expected to be small for a wall-resolved DNS.

B. DNS results

In Fig.5 the Fauconnier's DNS is compared to our numerical results.

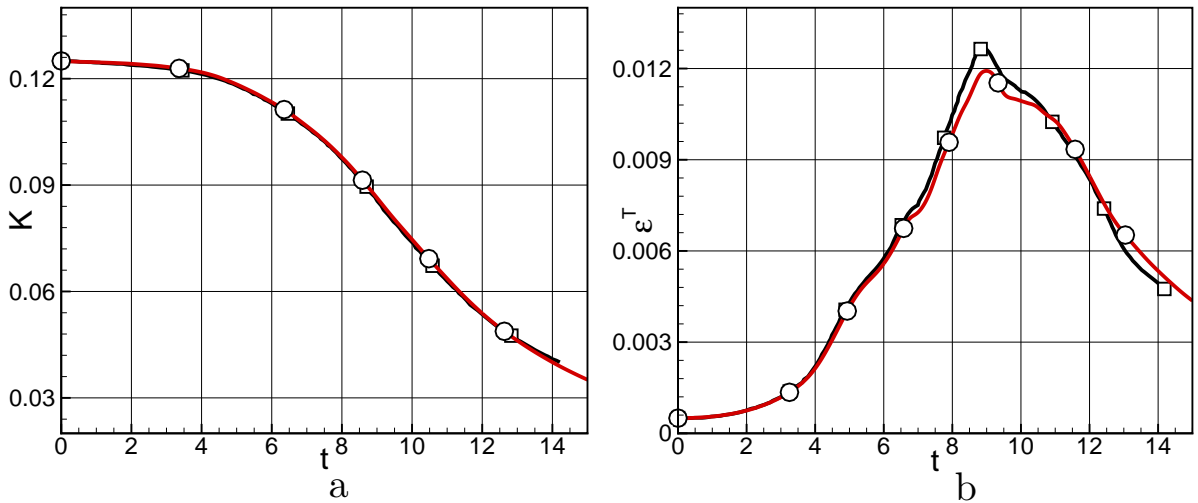


Figure 5. Time evolution of the kinetic energy (a) and of the total dissipation (b)(dimensionless variables). Fauconnier's DNS (\square —) and AETHER's DNS (\circ —)

At the initial time, K can be computed from the analytical solution $K = 0.125$ which is the value recovers by the simulation. At the beginning, turbulent structures are large vortices that lead to low dissipation. At $t = 2$, the structures start to break into smaller ones and the energy transfer from larger scales to smaller scales occurs. The kinetic energy starts to fall and the dissipation increases accordingly.

Three snapshots of the turbulent flow based on the λ_2 criterion of Jeong and Hussain (1995) [28] are displayed in Fig.6, and the transition to turbulence is clearly visible between Fig.6(a) and Fig.6(b). The dissipation is basically imposed by the larger scales of the flow, reaching a maximum at $t = 9$. A full energy cascade is then observed, and the flow finally vanishes thanks to the work of the molecular dissipation. It has been checked that ϵ^T is very close to ϵ^R . Moreover a good comparison is found with the DNS of Fauconnier.

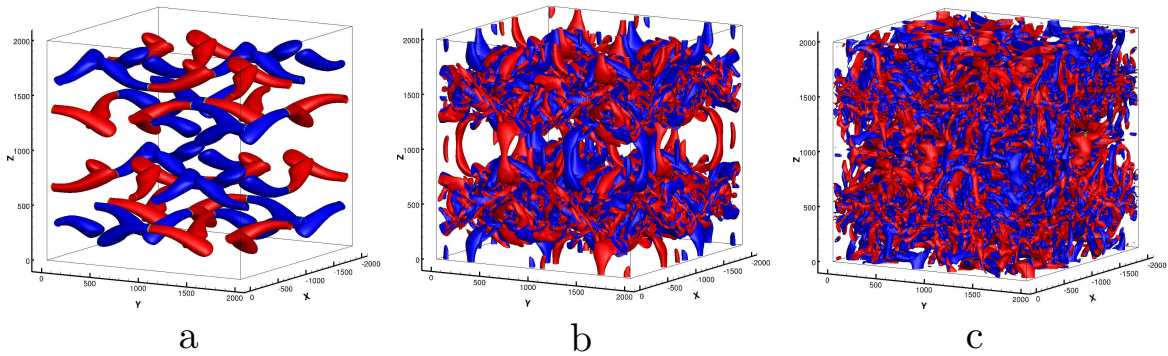


Figure 6. Flow structures calculated by DNS at $t = 2$ (a), at $t = 9$ (b) and at $t = 15$ (c). Vortical structures are shown using the λ_2 criterion for the value of $0.4 \times L_0/u_0$ coloured by the vorticity in the \underline{z} direction.

C. Validation of the VMS model

Our improved VMS model Eq.(3) is now compared to other LES models for the Taylor-Green flow. In Fig.7, the time evolution of the resolved dissipation ϵ^R is plotted for various models collected in Tab.1. The modelled dissipation ϵ'' is added in dotted lines for the computations made with AETHER code.

A	DNS results of Fauconnier, filtered on the LES mesh	□ —
B	LES with dynamic Smagorinsky model (Fourier space)	○ —
C	LES with Smagorinsky AETHER, finite element of order 3	△ —
D	LES with VMS model AETHER, finite element of order 3, Gaussian filter (order 3)	▽ —
E	LES with VMS model AETHER, finite element of order 3, interpolation filtering (order 2) (see section 1)	◇ —

Table 1. Models used for the Taylor-Green flow

The filtered DNS dissipation (A) has a lower dissipation peak because small structures are removed by the filtering process. The classical Smagorinsky model (C) is the lowest in term of resolved dissipation. The curve is separated at $t = 5$ from the DNS result. In fact, the Smagorinsky model dissipates the large structures. The first problem is that the modelled viscosity is too great because of its evaluation based on the resolved flow field. The second problem is that the model impacts all sizes of flow structures. The diffusive flux model is built on a resolved flow Laplacian. This can be explained by the flattest evolution of the resolved dissipation. Moreover, this argument is validated by comparing ϵ^R to ϵ'' . The curves have the same shape but are different in level which is expected. ϵ'' is indeed different from ϵ^R only by the scalar ν_t which is computed on the resolved field too. This similar evolution means that the Smagorinsky model is triggered by the whole wave numbers of the spectrum. The dynamic Smagorinsky resolved dissipation (B) is still lower than the filtered DNS one. But the dynamic method tends to improve the classical Smagorinsky result. Indeed, the first problem of the Smagorinsky model is addressed by adapting the turbulent viscosity to the flow by a filtering approach (see Germano [16]).

The first VMS model (D) succeeds to simulate accurately the resolved dissipation. Thanks to the filtering process, the VMS adapts dynamically the turbulent viscosity and above all changes the Smagorinsky spectral effects. The benefit obtained by addressing the second problem of the classical Smagorinsky leads to a better improvement on the flow simulation. This VMS result is computed with a global inversion of the filtering matrix which leads to a well resolved filtered solution. The VMS modelled dissipation ϵ'' is 100 times lower than the Smagorinsky one. Nonetheless its dynamics strictly follows the time events of the Taylor-Green vortices described by Brachet *et al* [3] and identified by Fauconnier [14]. The model stands still to zero until the first step around $t = 7$. The vortex flow becomes heavily distorted which may be interpreted as flow turbulence and thus model activation. The second event occurs around $t = 8$ where the flow break-down

begins. Then the model reacts intensively to the dissipation peak at $t = 9$.

The second VMS model (E) gives satisfying results. The resolved dissipation is merely the same with the first VMS model. The real difference can be seen on the model dissipation. On one hand, the first VMS (D) is equivalent to a well order 3 resolved filtering equation. On the other hand, the second VMS (E) is simplified to suit industrial needs and are equivalent to an order 2 filtering equation. For an order of magnitude, the simulation cost is 20 times lower for the second VMS computation. The differences can be explained by two effects which are links to the filtering process. First, the difference of amplitude is around a ratio of 10 which can be explained by the order of the filtering. Indeed, a greater filtering equation leads to a thinner structures selection for the model. Secondly, the flatter evolution of the second VMS is due to the numerical errors induced by the simplification of the filtering method. This leads to an inaccurate filtering selection of the wave numbers used in the second VMS model.

Nevertheless, the VMS (E) filtering process is chosen to test the near-wall treatment on LEISA II. Indeed, this is a good applicant in light of the balance between computing efficiency and accuracy.

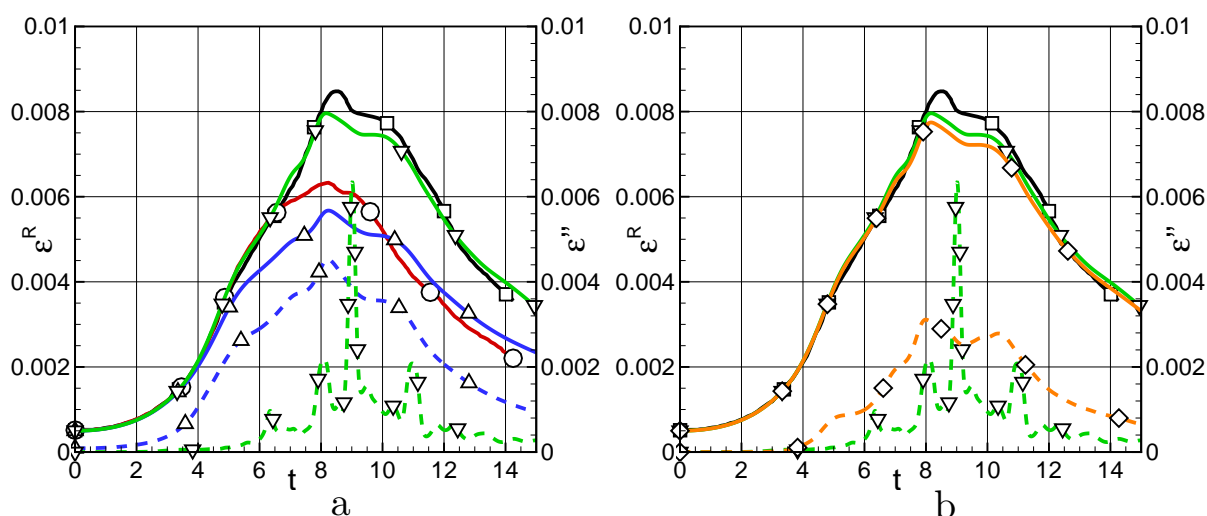


Figure 7. Time evolution of the resolved (—) and modelled dissipation (---). On the left A, B, C, D models. On the right A, D, E models. The VMS (D) modelled dissipation is multiplied by a factor 100 and the VMS (E) modelled dissipation by a factor 10.

In Fig.8 are plotted the spatial kinetic energy spectra in the volume for A, C and E. The VMS and Smagorinsky spectra follow the DNS one until the mesh cut-off wave number $k/k_{max} = 1/64 \simeq 0.15$. Each models show the kinetic energy cascade between $k/k_{max} \in [0.04, 0.6]$. The low waves numbers are not well resolved because of the spatial domain size. The VMS model is able to correctly transfer the energy without creating an energy pile-up called cusp near the cut-off wave number. This phenomenon could be induced by a wrong filtering method leading to a too low energy transfer (see Levasseur [29]). The DNS evolution near the end of the spectrum can be imputed to numerical errors and stabilisation method.

The VMS formulation developed in this study and implemented in a finite element algorithm, provides good results. This is possible thanks to a better spectral support of the model diffusive flux with respect to the other approaches, which consist mainly in changing the expression of the turbulent viscosity ν_t .

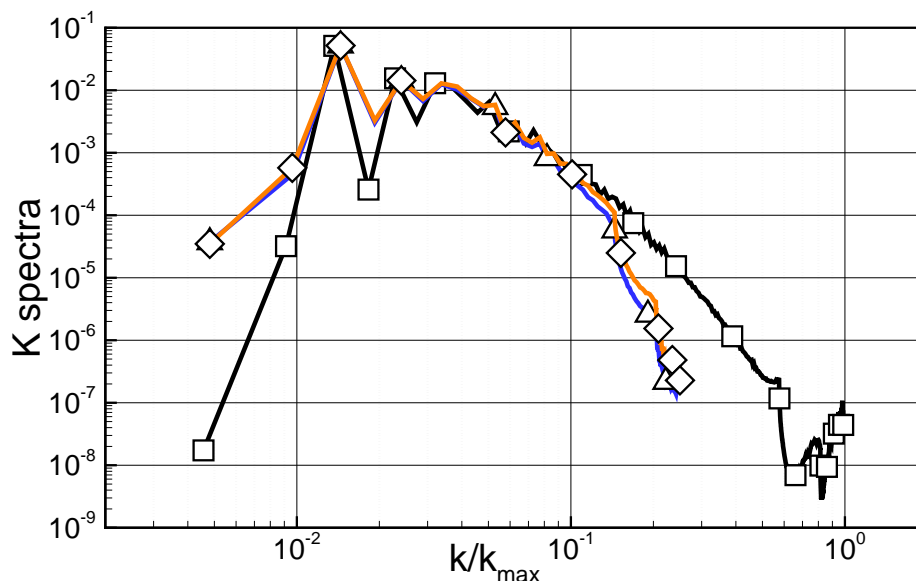


Figure 8. Spatial spectra of kinetic energy at $t = 10$ for AETHER DNS ($\square \text{ ---}$), VMS ($\diamond \text{ ---}$) and classical Smagorinsky ($\triangle \text{ ---}$)

IV. LEISA II benchmark

The LEISA II problem had been introduced by Manoha and Pott-Pollenske [33] as a benchmark for airframe noise computations for a high-lift wing, see Fig.9. It aims to provide experimental results in order to validate numerical codes used to compute and understand unsteady flow and noise generation near the slat at take-off and landing configurations. The experimental campaign was performed in two different wind-tunnels. First, the aerodynamic model had been adapted by the DLR in the F2 windtunnel at ONERA-Le Fauga. Then the acoustic measurements were performed in the anechoic open jet wind-tunnel AWB at DLR-Braunschweig. PIV, LDV, velocity correlations and spectra are available.

Interesting phenomena are observed on this problem, as the development of the shear layer between the slat and the main body, which requires an accurate description of the incoming boundary layer. This is first a nice benchmark problem to assess the behaviour of the present VMS model Eq.(3). An hybrid version of this model is also adapted in order to be able to work in DDES mode near the walls, see Eq.(4). Finally turbulent structures impact the upper inner side of the slat, and generate noise. The integral formulation of Curle (1955) [9] is used to compute the radiated far-field spectra.

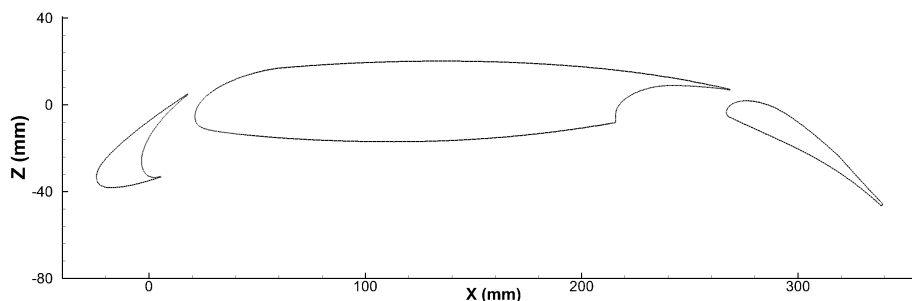


Figure 9. LEISA II 2D geometry

A. Numerical parameters

The geometrical configuration is the LEISA II profile (Fig.9) which has been extruded along the y axis from $y = 0$ mm to $y = 60$ mm. Periodic boundary conditions are applied in the spanwise direction. The spanwise

size of the computational domain is expected to contain at least two integral length scales. The in-flow conditions is provided by the LEISA II benchmark. The nominal parameters are the pressure $P_0 = 100136$ Pa, the Mach number $M_\infty = 0.1804$, the temperature $T_0 = 289.45$ K and the angle of attack $\alpha = 6.15^\circ$. The Reynolds number based on the reference chord $C = 300$ mm is $Re_C = CU_\infty/\nu = 1.2 \times 10^6$ where $u_\infty = M_\infty \times c_0$ and c_0 the sound velocity.

In order to keep a reasonable mesh size, the flow around the slat is privileged in terms of node density. One of the main goals of this simulation is to catch physics and validate our hybrid model in this area. The mesh in the transverse direction is regular with a step size of $\Delta y = 0.5$ mm. In the x and z axis, the mesh is fully unstructured. The elements are tetrahedric and of order 3 that is with a spatial quadratic interpolation. Three areas with distinct mesh sizes have been defined, see Fig.10. The first area is designed to have an average length scale of $\Delta x = \Delta z = 0.2$ mm. The second area following the shear flow between the slat and the wing is designed to satisfy an average length scale of $\Delta x = \Delta z = 0.15$ mm. Finally, the third area located around the trailing edge of the lower part of the slat has an average scale of $\Delta x = \Delta z = 0.1$ mm. The final spatial order 3 mesh is made of 35.10^6 degrees of freedom and 26.10^6 of elements. The time step is taken equals to 7.0×10^{-7} seconds.

The mesh properties are summarized in Tab.2 where the subscript *ref* represents the area of interest between the slat and the wing, Δx_{ref}^i is the mean length scale in a transverse plane of the subarea described above, Δy_{ref} is the length scale along the y axis and Δn_{min} is the distance of the closest point from the wall.

N	Spatial order	Δx_{ref}^1	Δx_{ref}^2	Δx_{ref}^3	Δy_{ref}	Δn_{min}	Model
[10^6]	/	C*[10^{-4}]	C*[10^{-4}]	C*[10^{-4}]	C*[10^{-4}]	C*[10^{-4}]	/
35	3	6.66	5.00	3.33	16.66	0.05	VMS

Table 2. Mesh properties used in LEISA II benchmark

The simulation is performed with the AETHER code with the hybrid VMS method Eq.(3) whereas the near-wall flow is computed with the Spalart DDES method. A *Reynolds Averaged Navier Stokes* (RANS) simulation is carried out in order to initiate the unsteady computation. An unsteady VMS computation is then done during 12.5 convected time C/u_∞ in order to evacuate all the transient regime. Finally, the data are recorded during 85 ms corresponding to roughly 18 convected times.

B. Overview of the turbulent flow

The turbulent kinetic energy $k_t = (\overline{u'^2} + \overline{v'^2} + \overline{w'^2})/2$ is plotted in Fig.11. This quantity underlines the turbulent production which is concentrated along the shear layer and around the impact area. The circulation flow inside of the slat cavity is also visible.

Fig.11(b) displays a Schlieren snapshot illustrating the turbulent development. The Schlieren field is computed by $\|\nabla \rho\|$. On the early stage of the lower shear layer, Kelvin-Helmholtz vortices develops. These coherent structures are convected until a breakdown occurs inside the slat cavity. The Schlieren view appears to be more diffusive, meaning that higher wave number structures are present in the flow. These structures are dragged in part by the cavity recirculation, but the large part is sucked by the upper shear layer.

The turbulent viscosity field inside the slat cavity is plotted in Fig.12(a). The superscript T is defined as $\nu_{VMS}^T/\nu - 1 = (\nu_{VMS} + \nu)/\nu - 1 = \nu_{VMS}/\nu$. The protection area of the DDES, refer to Eq.(4), can be easily seen on the upper side of the slat. The turbulent viscosity field is directly linked to the velocity gradients as expected, but its value is smartly activated by the VMS model.

The ratio between the viscosity provided by VMS and DES is plotted in Fig.12(b). DDES area disappears and only a thin zone of transition between VMS and DES remains on the outer upper side of the slat. Away from the slat, the VMS viscosity is lower than the DES-Smagorinsky which is expected from model behaviour. In the slat cavity and the shear layer regions, the VMS viscosity takes however higher values than the Smagorinsky model especially in areas of intense shear flows.

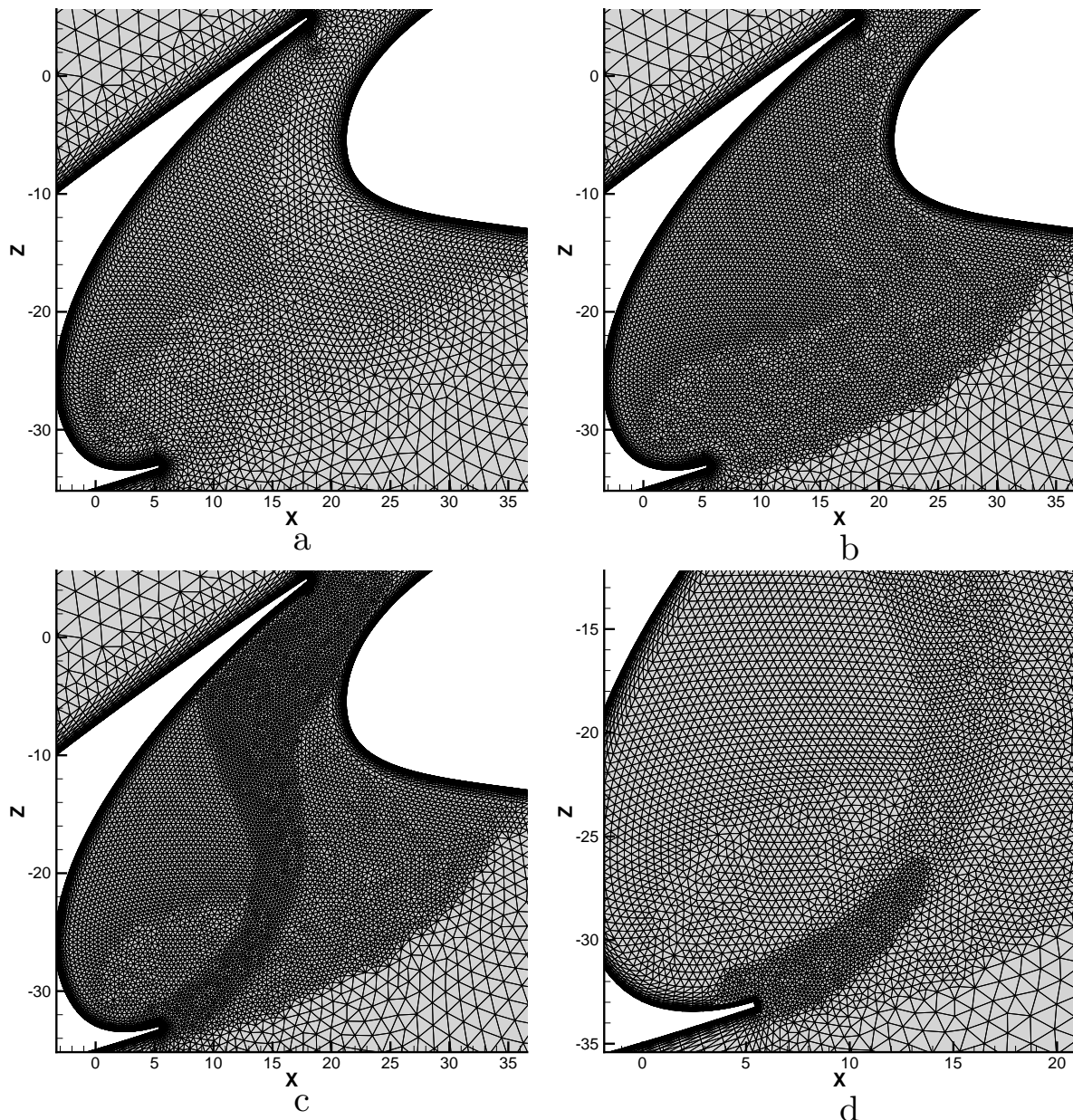


Figure 10. Mesh building steps near the slat region : (a) initial mesh (b) isotropic homogenisation, (c) refinement in the shear layer and (d) refinement near the slat trailing edge.

It appears interesting to examine the filtered field of the velocity in order to understand the behaviour of the filtering part of the VMS model. The filtered longitudinal velocity is shown in Fig.13. The protected area of the boundary layer can be again clearly observed. The filtered field captures areas of intense turbulent activities. For instance, both shear layers and cavity are filled with structures. Moreover the model selects only these zones when others remains untouched.

It is possible to draw the quantities which are used to inform each model. These quantities are the gradient of the velocity for the DES-Smagorinsky and the gradient of the filtered velocity for the VMS. In Fig.14(a), the DES-Smagorinsky model is activated in the outer area of the cavity slat showing large blue and red zones. This activation is linked to the diffusion induced by the Smagorinsky model from the large scales. The structures in the cavity are as thin as in Fig.13 because each snapshot represents a norm of the velocity gradient. The smart effect of the VMS filtering process is illustrated in Fig.14(b). First the Laplacian equivalent norm of the gradient filtered velocity selects thinner size structures in the cavity. Furthermore only areas where the viscosity model needs to be applied are selected. The low wave numbers

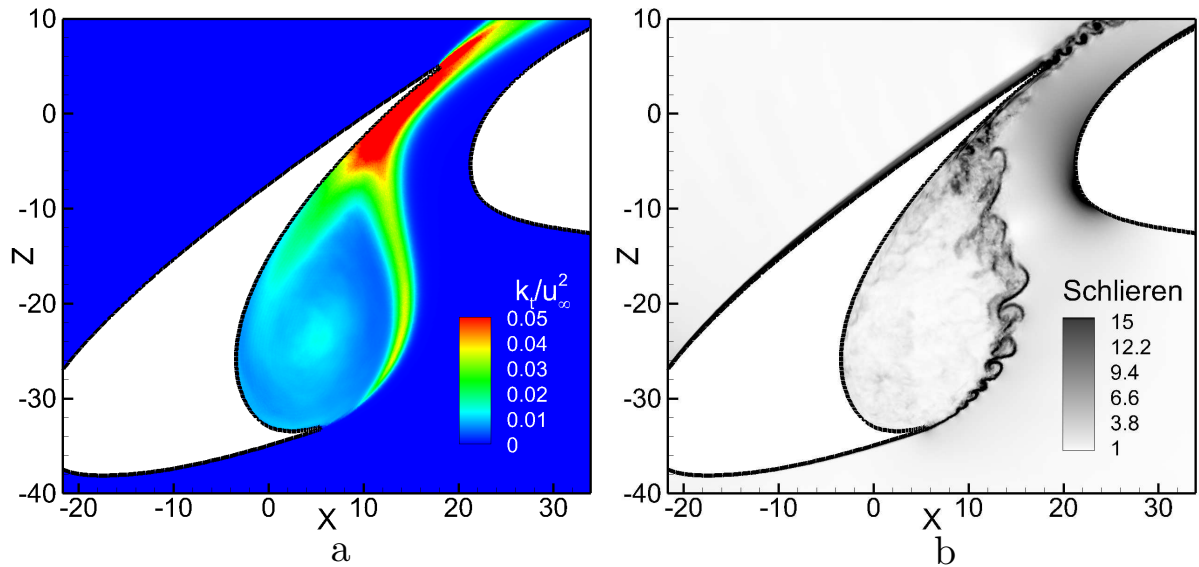


Figure 11. On the left : turbulent kinetic energy field. On the right : snapshot of the Schlieren

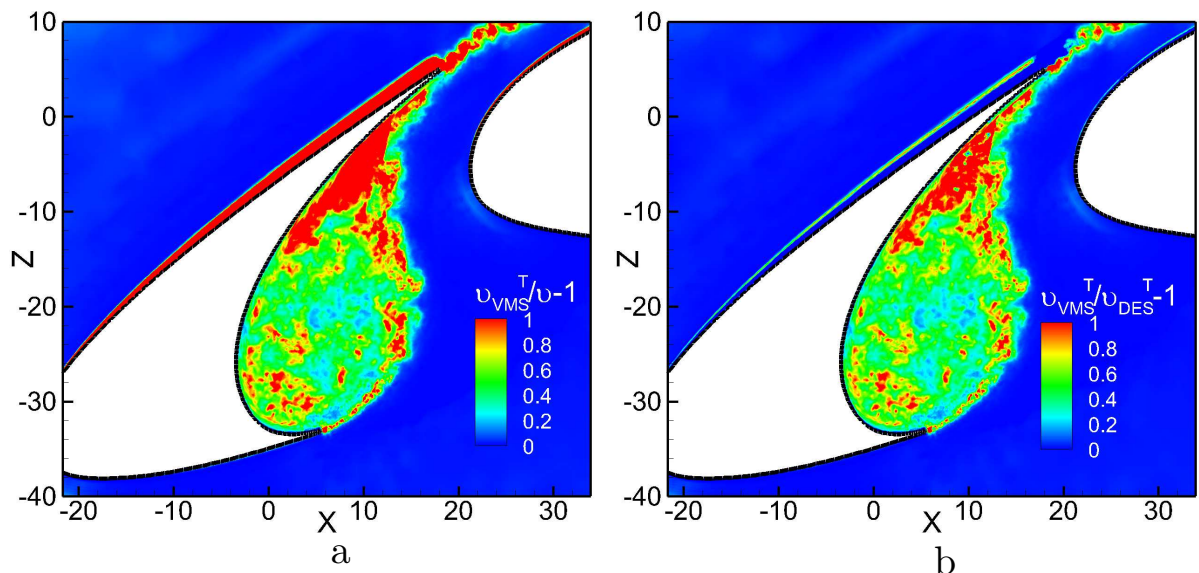


Figure 12. On the left : VMS turbulent viscosity. On the right : VMS turbulent viscosity compared to the turbulent viscosity of DDES model. Superscript T represents the sum with the molecular viscosity

are thus not impacted by the modelling in contrast to the classical Smagorinsky model.

C. Near-wall model

The study of the quantities near the wall helps to understand the activation and transition in the hybrid model. The pressure coefficient C_p gives information on the mean flow computation. The pressure coefficient is plotted in Fig.15. The numerical simulation fits well the experiment curve on all the profile except for the outer side of the slat. It appears that the flow solution is very sensitive to the value of the angle of attack. The present experimental data can be recovered with RANS simulations by chosen $\alpha \simeq 5.85^\circ$ for instance. This is a difficulty in order to compare experimental and numerical data especially concerning the probes. In some areas, the numerical probes won't see the same flow as the experiment ones. For instance see the position of the experimental probe 11108-5-2 in Fig.16.

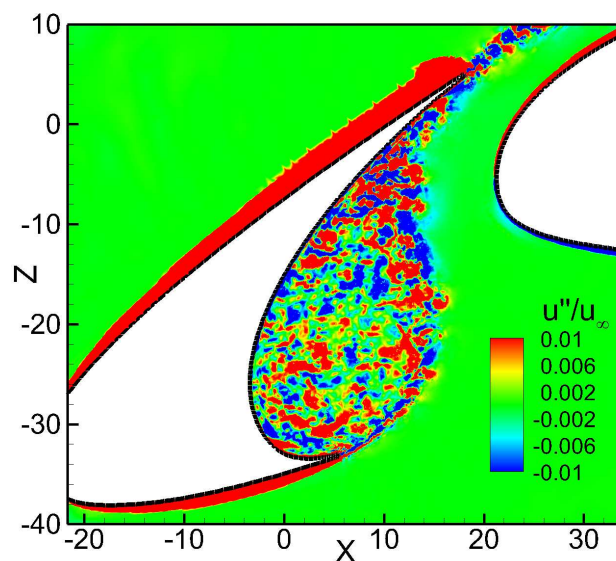


Figure 13. Snapshot of the filtered longitudinal velocity field u'' for the VMS model

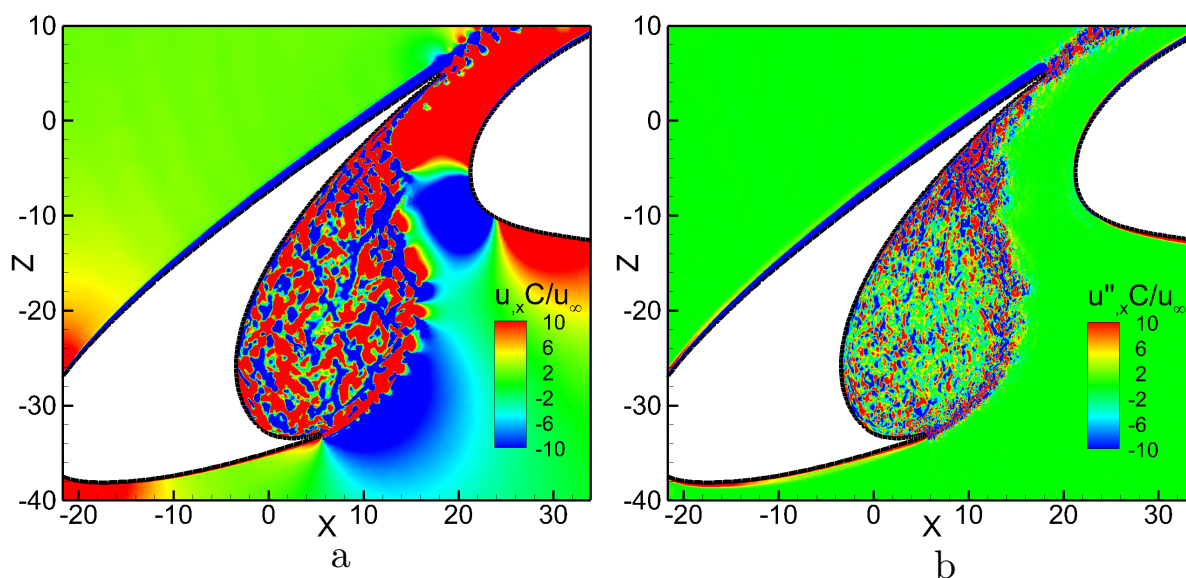


Figure 14. Snapshot of $\partial u/\partial x$ used as input in the DDES-Smagorinsky model (on the left) and $\partial u''/\partial x$ for the VMS model (on the right)

The velocity is recorded at three positions 1 to 3 located nearer to the trailing edge of the slat outer lower part. In Fig.17(a), the velocity profiles follow a typical laminar boundary layer law until a flat evolution outside it. The value of the curve plateau decreases along the position like a classical NACA (see Marsden *et al* [34]).

The picture Fig.17(b) shows the evolution of the hybrid model quantities. The clipping function f_d is plotted and slowly rise until the unity. The evolution of the clipped u_{vms}^+ follows the evolution of u^+ until $y^+ = 10$ where the fluctuations of VMS are slowly introduced. The value of u_{vms}^+ is 50 times lower than the other quantities which is the order of magnitude of fluctuations near the wall. In fact u_{vms}^+ represents fluctuations too. This study of near wall mesh area validates the effect of the VMS hybrid approach. It can introduce fluctuations in the URANS area without damaging the velocity field of the boundary layer.

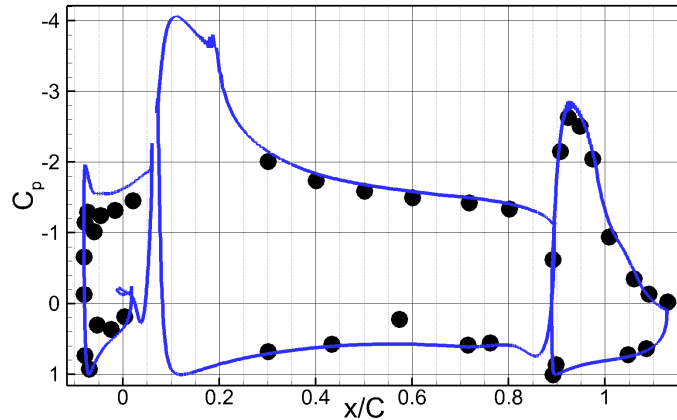


Figure 15. Pressure coefficient at the wall

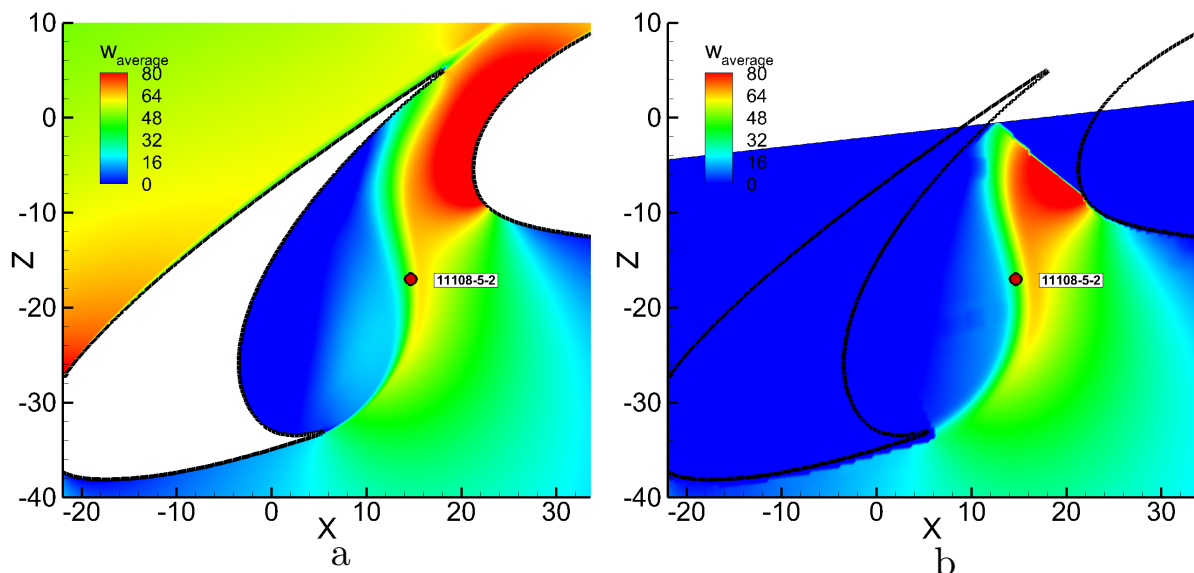


Figure 16. Comparison of $w_{average}$ field in the cavity between computation and experiment. The probe 11108-5-2 is not in the same flow in (a) (Simulation) and (b) (Experiment PIV)

D. Spectra

The VMS model acts on the spectrum in order to have a good agreement with the energy transfer both in high and low frequencies. Thus the velocity spectra need to be plotted in order to check the effect of the VMS model. But because of the angle of attack problem raised above, the comparison in the shear layer is more difficult. The end of the shear layer is thicker which allows to have an easier comparison. Thus the experimental probe 11108-9-2 just before the impact is chosen. The position and the longitudinal velocity spectrum are plotted in Fig.18. The numerical spectrum shows a good agreement with the experimental probe, both in high and low frequencies. The inflection frequency of the curves is located around $f = 5000$ Hz.

The evolution of the spectrum along the shear layer is plotted in Fig.19. The position of each steps are shown in Fig.19(a). At the beginning of the shear layer, the Kelvin-Helmholtz frequency is visible at $f = 3000$ Hz. This instability frequency can be recovered by the work of Galdeano [15] done on the LEISA I benchmark. The wave length of shear layer instability created by two flows convected in the same direction are given by

$$\lambda_a = 28 * \delta_0$$

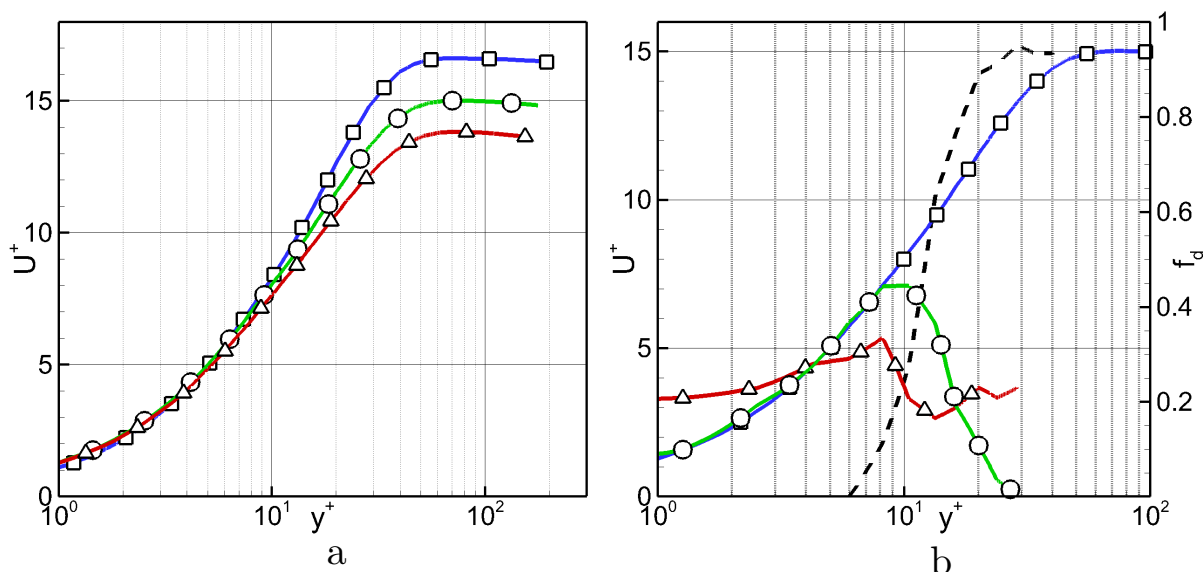


Figure 17. Velocity profile (a) plotted in wall units. Positions 1 (\square —), 2 (\circ —) and 3 (Δ —) respectively nearer to the lower trailing edge. Evolution of the hybrid method near the wall at position 2 : clipping function f_d (---), u^+ (\square —), $u_{vms}^+ * 50$ (Δ —) and clipped u_{vms}^+ evolution (\circ —)

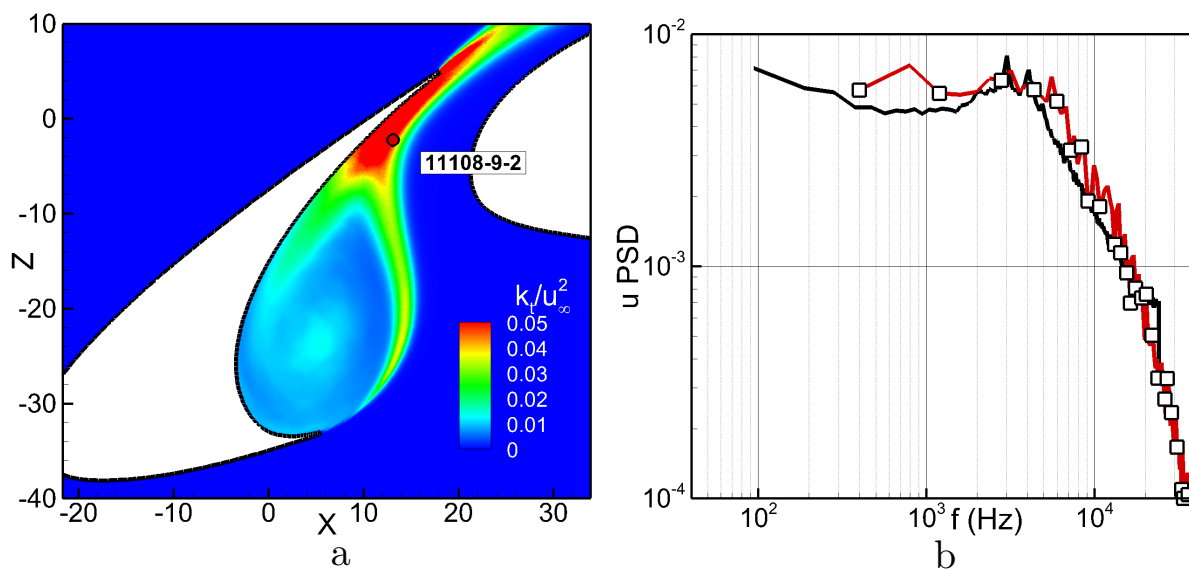


Figure 18. PSD of longitudinal velocity at probe 11108-9-2 (b). Experiment (—) and VMS (\square —). Position of the probes 11108-9-2 on the left (a)

where $\delta_0 = 0.4$ mm is the width of the shear layer in this study. The history evolution of the spectrum can be compared to the picture of the Schlieren snapshot in Fig.11(b). The energy of this instability increases along the shear layer until the Kelvin-Helmholtz vortices are well visible. The peak becomes thicker and highlights the shape structures in the flow. Then the vortices are combined and increased the low frequency level of the spectrum. A lot of different structure sizes are then present in the flow, leading to a flatter spectrum and a more fuzzy cloud of Schlieren quantity. At the $2/3$ of this shear layer, the curve tends to a classical spectrum of an homogenous isotropic turbulence with a $k^{-5/3}$ slope for the cascade.

The final comparison between experiment versus modelling is on the aero-acoustic propagation in far field. The microphone used for this comparison is the fourth, right under the profile. The pressure is dimensionless using $p_{ref} = 2.10^{-5}$ Pa. The several VMS peaks are well computed compared to F2 and AWB experiment. But the spectrum dynamics is different from F2 to AWB results. The VMS spectrum energy is closer to

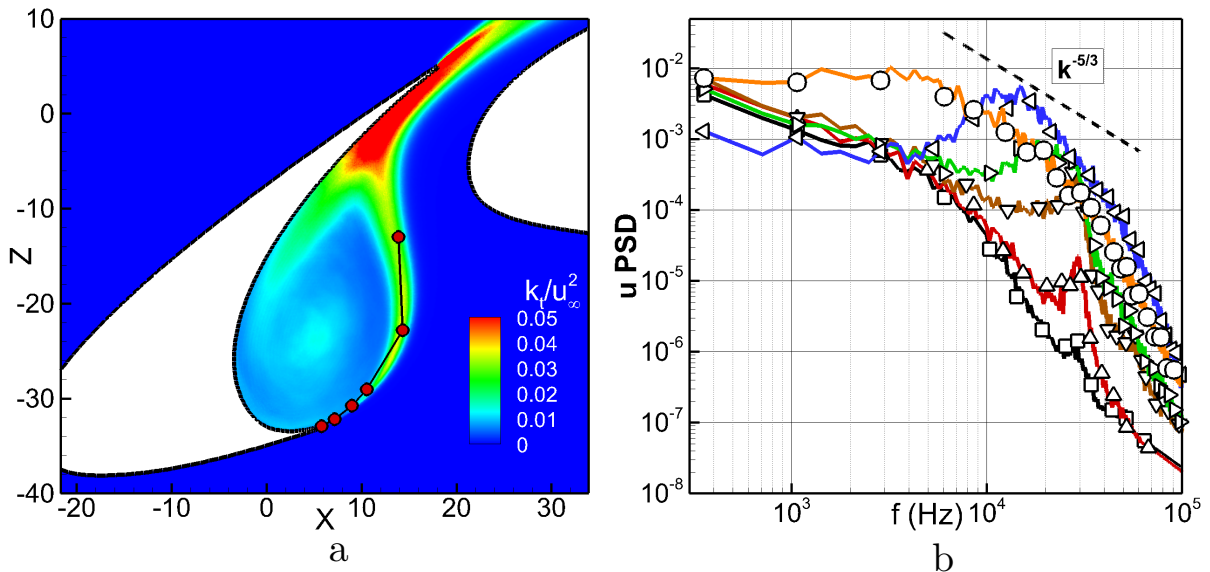


Figure 19. Evolution of the longitudinal velocity spectrum along the shear layer. (a) Position of the probes. (b) Velocity spectra along the shear layer respectively \square —, Δ —, ∇ —, \triangleright —, \triangleleft — and \circ — and $k^{-5/3}$ slope curve - - -

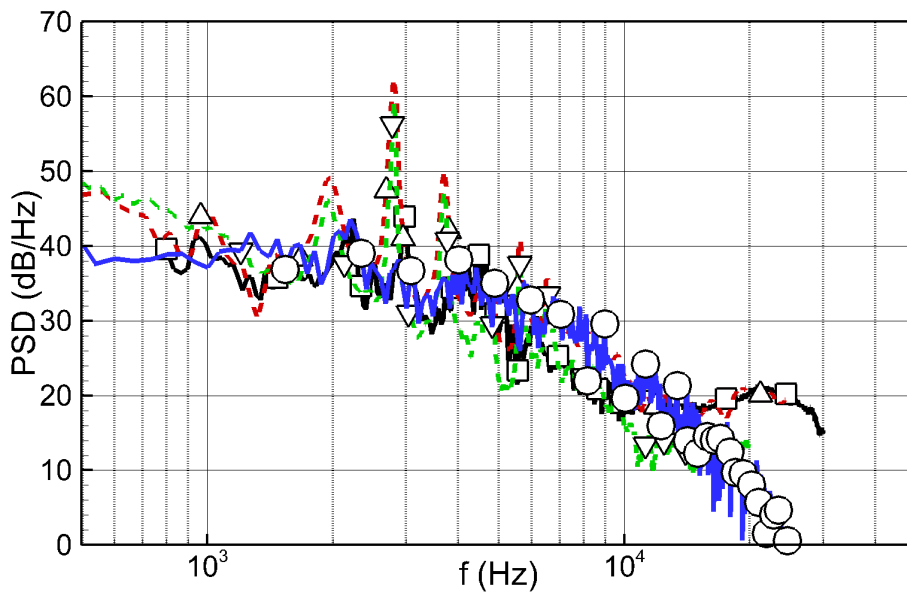


Figure 20. Pressure PSD on microphone 4 : F2 (\square —), AWB Onera (Δ - - -), AWB DLR (∇ - . -) and VMS AETHER (\circ —)

the F2 result. Globally VMS simulation is closer to F2 results both in energy and frequency. The spectrum shows tonal peaks at $f = 2000$ Hz and $f = 3000$ Hz and a wide acoustic activity around $f = 4000$ Hz.

V. Conclusion

In this study a high-order VMS subgrid model has been presented. Its formulation is well suited to be combined with a finite element algorithm written for entropic variables and a SUPG stabilisation method. The chosen filtering procedure appears to be efficient for Lagrangian elements in terms of numerical costs and flow modelling. This is especially true for iso-parametrical and symmetrical elements. Moreover the hybrid approach can couple the VMS model with different DES methods.

The Taylor-Green vortex flow has highlighted the problem of the Smagorinsky subgrid-scale model used in several DDES approaches. The low frequency part of the kinetic energy spectrum is impacted by the subgrid diffusive flux. The VMS model has addressed this problem by a proper explicit filtering.

The LEISA II computation allows to validate this hybrid VMS method on a complex flow. The filtered field is promising and selects the right flow areas to applied the VMS model. Furthermore, the hybrid approach has the expected effects and doesn't degrade the nearest wall areas. The VMS hybrid approach predicts good results in terms of spectral evolution both in flow and acoustic computation.

The present work is still in progress.

Acknowledgments

The thesis of Pierre Yser is funded by the French ANRT and the aircraft maker Dassault Aviation (Saint-Cloud, France). All the computations were made thanks to the HPC resources from Dassault Aviation cluster.

References

- ¹C. Bailly and G. Comte-Bellot. *Turbulence*, volume ISBN 978-3-319-16159-4. Springer, 2015.
- ²C. Bogey and C. Bailly. Decrease of the effective reynolds number with eddy-viscosity subgrid-scale modelling. *AIAA Journal*, 43(2), 2005.
- ³M. Brachet, D. Meiron, S. Orszag, B. Nickel, R. Morf, and U. Frisch. Small-scale structure of the taylor-green vortex. *J. Fluid. Mech.*, 130, 1983.
- ⁴M. J. Brazell, A. Kirby, M. Stoellinger, and D. J. Mavriplis. Using les in a discontinuous galerkin method with constant and dynamic sgs models. AIAA, 5-9 January AIAA 2015.
- ⁵G. Carey and J. Oden. *Finite elements : A second course*, volume volume II. Prentice-Hall, 1983.
- ⁶F. Chalot, F. Dagrau, M. Mallet, P. Normand, and P. Yser. Higher-order rans and des in an industrial stabilized finite element code. *Contribution of Dassault Aviation to the IDIHOM Project*, 2014.
- ⁷F. Chalot, V. Levasseur, M. Mallet, G. Petit, and N. Reau. Les and des simulations for aircraft design. 0723, January 2007.
- ⁸F. Chalot and P.-E. Normand. Towards high-fidelity industrial cfd. *Computational Fluid Dynamics*, June 14-17 2010.
- ⁹N. Curle. The influence of solid boundaries upon aerodynamic sound. Proceedings of the Royal Society of London, 1955.
- ¹⁰E. David. *Modélisation des écoulements compressibles et hypersoniques : une approche instationnaire*. PhD thesis, I.N.P. de Grenoble, 1993.
- ¹¹S. Deck. Recent improvements in zonal detached eddy simulation(zdes) formulation. *Theoretical and computational fluid dynamics*, September 2011.
- ¹²L. T. Diosady and S. M. Murman. Higher-order methods for compressible turbulent flows using entropy variables. AIAA, 5-9 January 2015.
- ¹³G. Erlebacher, M. Y. Hussaini, C. G. Speziale, and T. A. Zang. Toward the large eddy simulation of compressible turbulent flow. *Journal of Fluid Mechanics*, 238, 1992.
- ¹⁴D. Fauconnier. *Development of a Dynamic Finite Difference Method for Large-Eddy simulation*. PhD thesis, Universiteit Gent, 2008-2009.
- ¹⁵S. Galdeano. *Simulation et localisation de sources aéroacoustiques autour de profils hypersustentés*. PhD thesis, Université Pierre et Marie Curie, Janvier 2013.
- ¹⁶M. Germano. Turbulence : the filtering approach. *Journal of Fluid Mechanics*, 238, 1992.
- ¹⁷M. Germano. *Fundamentals of Large-Eddy simulation*. Springer, 81-130 edition, 1998. (Advanced TurbulentFlows Computations, Peyret and Krause eds), CISM Courses and Lecture 395.
- ¹⁸M. Germano, U. Piomelli, P. Moin, and W. H. Cabot. A dynamic subgrid-scale effy viscosity model. *Phys. Fluids*, A 3(7), 1991.
- ¹⁹S. Ghosal. Mathematical and physical constraints on large-eddy simulation of turbulence. *AIAA Journal*, 37(4), 1999.
- ²⁰M. C. Hsu, Y. Bazilevs, V. M. Calo, T. E. Tezduyar, and T. J. R. Hughes. Improving stability of stabilized and multiscale formulations in flow simulations at small time steps. *Computer methods in applied mechanics and engineering*, (199), 2010.
- ²¹T. Hughes. *The finite element method : Linear Static and Dynamic Finite Element Analysis*. Prentice-Hall, 1987.

- ²²T. Hughes, L. P. Franca, and G. M. Hulbert. A new finite element formulation for computational fluid dynamics : Viii. the galerkin/least-squares method for advective-diffusive equations. *Computer methods in applied mechanics and engineering*, (73), 1989.
- ²³T. Hughes, L. Mazzei, and K. E. Jansen. Large-eddy simulation and the variational multiscale method. *Comput. Visual. Sci.*, 3:47–59, 2000.
- ²⁴T. Hughes, A. A. Oberai, and L. Mazzei. Large-eddy simulation and the variational multiscale method. *Phys. Fluids.*, 2001.
- ²⁵T. J. Hughes, L. Mazzei, and K. E. Jansen. Large-eddy simulation and the variational multiscale method. *Computing and Visualization in Science*, 3, 1999.
- ²⁶T. J. Hughes, L. Mazzei, A. A. Oberai, and A. A. Wray. The multiscale formulation of large eddy simulation : Decay of homogeneous isotropic turbulence. *Phys. Fluids.*, 13(2), 2000.
- ²⁷E. Itam, S. Wornom, B. Koobus, and A. Dervieux. Application of a hybrid variational multiscale model to massively separated flows. *50th 3AF*, 2015. Toulouse, France.
- ²⁸J. Jeong and F. Hussain. On the identification of a vortex. *J. Fluid. Mech.*, 285, 1995.
- ²⁹V. Levasseur. *Simulation grandes échelles en éléments finis stabilisés : une approche variationnelle multi-échelles*. PhD thesis, Université Paris VI Pierre et Marie Curie, 2007.
- ³⁰D. Lilly. On the application of the eddy-viscosity concept in the inertial subrange of turbulence. *Technical report*, 2006. Boulder, Colorado.
- ³¹T. S. Lund. The use of explicit filters in large eddy simulation. *Computers and Mathematics with Applications*, 46, 2003.
- ³²M. Mallet. *A finite element method for computational fluid dynamics*. PhD thesis, Stanford, 1985.
- ³³E. Manoha and M. Pott-Pollenske. Leisa 2 : an experimental database for the validation of numerical predictions of slat unsteady flow and noise. *AIAA 21st AIAA/CEAS Aeroacoustics Conference*, 22-26 June 2015.
- ³⁴O. Marsden, C. Bogey, and C. Bailly. Direct noise computation of the turbulent flow around a zero-incidence airfoil. *AIAA Journal*, 46(4), April 2008.
- ³⁵A. Najafi-Yazdi, M. Najafi-Yazdi, and L. Mongeau. A high resolution differential filter for large eddy simulation : Toward explicit filtering on unstructured grids. *Journal of Computational Physics*, 292, 2015.
- ³⁶N. Nikitin, F. Nicoud, B. Wasistho, K. Squires, and P. Spalart. An approach to wall modeling in large-eddy simulations. *Physics of Fluids*, July 2000.
- ³⁷P. Sagaut. *Large Eddy simulation for incompressible flows : an introduction*. Springer Berlin Heidelberg, 2 edition, 1998.
- ³⁸P. Sagaut, S. Deck, and M. Terracol. *Multiscale and Multiresolution Approaches in Turbulence*. Imperial College Press, 2006.
- ³⁹F. Shakib. *Finite element analysis of the compressible Euler and Navier-Stokes equations*. PhD thesis, Stanford, 1988.
- ⁴⁰M. L. Shur, P. R. Spalart, M. K. Strelets, and A. K. Travin. An enhanced version of des with rapid transition from rans to les in separated flows. *Flow Turbulence Combust*, May 2015.
- ⁴¹J. Smagorinsky. General circulation experiments with the primitive equations, the basic experiment. *Mon. Weather Rev.*, 92, 1963.
- ⁴²P. Spalart, S. Deck, M. Shur, K. Squires, M. K. Strelets, and A. Travin. A new version of detached-eddy simulation, resistant to ambiguous grid densities. *Theoretical and computational fluid dynamics*, May 2005.
- ⁴³P. Spalart, W. Jou, M. Strelets, and S. Allmaras. Comments on the feasibility of les for wings and on a hybrid rans/les approach. Proceedings of the 1st AFOSR Int. Conf. on DNS/LES, 1997.
- ⁴⁴G. Strang and G. Fix. *An analysis of the finite element method*. Prentice-Hall, 1973.
- ⁴⁵J. C. Uribe, N. Jarrin, R. Prosser, and D. Laurence. Development of a two-velocities hybrid rans-les model and its application to a trailing edge flow. *Flow turbulence Combust*, 2010.
- ⁴⁶B. Vreman, B. Geurts, and H. Kuerten. A priori tests of large eddy simulation of the compressible plane mixing layer. *J. Eng. Mathematics*, 29, 1995.
- ⁴⁷O. V. Vasilyev, T. S. Lund, and P. Moin. A general class of commutative filters for les in complex geometries. *Journal of Computational Physics*, 146:82–104, July 1998.
- ⁴⁸H. Xiao and P. Jenny. A consistent dual-mesh framework for hybrid les/rans modeling. *Journal of Computational Physics*, 2012.
- ⁴⁹P. Yser, S. Barre, F. Chalot, and F. Dagrau. High-order and subgrid model effects on finite elements des-les computations of a transonic cavity experiment. *3AF*, March 30-April 1, 2015.
- ⁵⁰O. Zienkiewicz. *The Finite Element Method*. London : McGraw-Hill, 1977.